Diblock Copolymers of Ethylene Oxide and 1,2-Butylene Oxide in Aqueous Solution. Effect of E-Block-Length Distribution on Self-Association Properties

Ga-er Yu, Zhuo Yang, Mahmoud Ameri, David Attwood, John H. Collett, Colin Price, and Colin Booth*

Departments of Chemistry and Pharmacy, Manchester Polymer Centre, University of Manchester, Manchester M13 9PL, UK

Received: February 14, 1997; In Final Form: March 25, 1997[⊗]

Block copolymers were prepared by copolymerization of ethylene oxide and butylene oxide to have identical overall composition and chain length but to differ in their distributions of oxyethylene (E) block length by virtue of the sequence of polymerization of the two monomers: ethylene oxide first to obtain copolymer $E_{41}B_8$, and butylene oxide first to obtain B_8E_{41}. Gel permeation chromatography was used to show that the chain length distributions were in accord with the prediction of the kinetic scheme of Weibull and Nycander. The effect of E-block-length distribution on the self-association (micellization) of the two copolymers in water was determined by means of surface tension and light scattering (dynamic and static) measurements. Compared with copolymer $E_{41}B_8$ under similar conditions, it was found that copolymer B_8E_{41} micellized more readily and formed larger micelles. The effect of the difference in micellar properties on the gelation of moderately concentrated solutions of the two copolymers is described and discussed.

1. Introduction

Interest in the aqueous solution properties of a new family of block copolymer surfactants made from ethylene oxide (EO) and 1,2-butylene oxide (BO), members of which are distributed commercially by the Dow Chemical Company,[1] arises from the high hydrophobicity of the oxybutylene unit [B, $OCH_2CH(C_2H_5)$], which is about 4 times that of an oxypropylene unit [P, $OCH_2CH(CH_3)$], *e.g.*, in Pluronic surfactants.[2] As a consequence, comparable performance properties are achieved with oxyethylene/oxybutylene copolymers (E/B, E = OCH_2CH_2) of relatively modest molar mass, typically 2000−3000 g mol^{-1}: see recent reviews.[3] Work has included comparisons of self-assembly in aqueous solutions of linear diblock (E_mB_n), linear triblock ($E_mB_nE_m$ and $B_nE_mB_n$), and cyclic diblock (*cyclo*-B_nE_n) copolymers.[2,4−9] A feature of the work, emphasized in recent papers,[5,6,10] has been the effect on properties of the broad composition distributions of $E_mB_nE_m$ and B_mE_n copolymers prepared by sequential anionic polymerization of BO followed by EO. As pointed out by Nace *et al*.,[11] this is because of the large difference in reactivity of EO with primary E oxyanions compared with secondary B oxyanions. The effect on properties is particularly severe if E-block lengths are 30−40 units or less,[5,6] which is often the case for E/B copolymers.

$E_mB_nE_m$ triblock copolymers are prepared by polymerization of BO followed by EO, and it is awkward to prepare such copolymers *via* polymerization in the reverse sequence. However, diblock copolymers can be readily prepared using either sequence. In the present work the aqueous solution properties of diblock copolymer $E_{41}B_8$, prepared by sequential copolymerization of EO followed by BO, and so with narrow block length distributions of both components, are compared with those of diblock copolymer B_8E_{41} prepared by sequential copolymerization of BO followed by EO, and so with a relatively wide E-block-length distribution. Copolymer B_8E_{41} has been used in previous investigations of self-assembly[4,10] and of adsorption at hydrophobic surfaces,[12] and the phase diagram for copolymer $E_{41}B_8$ in water has recently been determined.[13] In this paper we report for the first time light scattering and surface tension measurements for aqueous solutions of copolymer $E_{41}B_8$. For purposes of strict comparison, further measurements were carried out for solutions of copolymer B_8E_{41} under identical conditions.

2. Experimental Section

2.1. Preparation of the Copolymer. The preparation of copolymer B_8E_{41} has been described previously.[4] Copolymer $E_{41}B_8$ was prepared by sequential polymerization of EO followed by BO as follows. 2-(2-Methoxyethoxy)ethanol ($CH_3OCH_2CH_2OCH_2CH_2OH$) was reacted with freshly cut potassium metal to form a solution of its salt ($OH/K^+ \approx 15$). A portion of this initiator solution was injected by syringe under dry-nitrogen flow into a previously-flamed ampule fitted with a Teflon tap, and the required amount of EO transferred in *via* a vacuum line. The ampule was immersed in a water bath at 45 °C for 1 week, and then at 65 °C until all EO was polymerized. The required amount of BO was then transferred into the ampule, which was left in the water bath at 65 °C for 1 week, then at 80 °C for 2 weeks. At each stage, total consumption of monomer was verified by cooling part of the ampule with a pellet of solid CO_2 and checking for condensation. Copolymer B_8E_{41} was purified by extraction with hexane, as described previously.[4,14] Copolymer $E_{41}B_8$ was sufficiently pure as prepared.

2.2. Gel Permeation Chromatography (GPC). The GPC system consisted of three PL-gel columns (two mixed B and one 500 Å). The eluent was tetrahydrofuran at 20 °C and flow rate of 1 cm^3 min^{-1}. A differential refractometer (Waters R410) was used to detect elution of sample. Elution volumes were referenced to dodecane as internal standard. Calibration was with poly(oxyethylene) standards.

GPC curves obtained for copolymers $E_{41}B_8$ and B_8E_{41} are shown in Figure 1. The difference in width of the two curves is apparent. The corresponding values of the molar mass ratio (M_w/M_n), which reflects the width of the number-distribution of molar mass, are 1.04 ($E_{41}B_8$) and 1.14 (B_8E_{41}), calculated from curves uncorrected for instrumental spreading. A differ-

[⊗] Abstract published in *Advance ACS Abstracts,* May 1, 1997.

S1089-5647(97)00570-1 CCC: $14.00

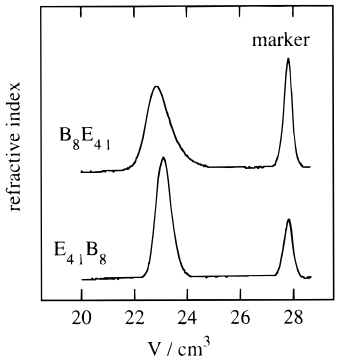

Figure 1. GPC curves for copolymers B_8E_{41} and $E_{41}B_8$ (as indicated). Elution volumes were referenced to dodecane as internal standard (marker).

TABLE 1: Molecular Characterization of the Copolymers

	GPC		^{13}C NMR		
copolymer	M_{pk}/ g mol^{-1}	M_w/M_n	M_n/ g mol^{-1}	mol % E	M_w[a]/ g mol^{-1}
$E_{41}B_8$	2400	1.04	2380	84	2480
B_8E_{41}	2700	1.14	2380	84	2710

[a] Calculated from M_n(NMR) and M_w/M_n(GPC).

ence in molar mass at the peak of the GPC curve (see Figure 1 and Table 1) was also found, which is qualitatively consistent with B_8E_{41} having the same number-average molar mass (M_n) but a broader molar-mass distribution. Quantitative comparison is made in section 3.

2.3. NMR Spectroscopy. NMR spectra were recorded by means of a Varian Unity 500 spectrometer operated at 500 MHz for ^{1}H or 125 MHz for ^{13}C spectra, using solutions of *ca*. 5 wt % in $CDCl_3$. Assignments for end and chain groups were taken from previous work.[15] Values of M_n (from end-group analysis) and composition (from chain-group analysis) obtained, listed in Table 1, were used to define the formulas of the copolymers.

2.4. Surface Tension. Surface tensions (γ) of dilute aqueous solutions were measured by detachment of a platinum ring suspended from a torsion balance (White Electrical Instrument Co. Ltd, England). The usual precautions were taken to ensure cleanliness, and the water was doubly-distilled and filtered (Millipore Millex-GS, Triton-free, 0.22 μm). The accuracy of measurement was checked by frequent determination of the surface tension of pure water. Solutions were held at the temperature of measurement ($\pm$0.2 °C) by means of a thermostated water jacket. The force of detachment was measured for different concentration solutions. Equilibrium was generally reached within 2 h to 2 days depending on concentration, the more dilute solutions needing the longer times.

2.5. Light Scattering. All glassware was washed with condensing acetone vapor before use. Solutions were clarified by filtering through Millipore Millex filters (Triton free, 0.22 μm porosity, sometimes 0.1 μm porosity) directly into the cleaned scattering cell.

Static light scattering (SLS) intensities were measured for solutions maintained at several temperatures in the range 25−50 °C by means of a Malvern PCS100 instrument with vertically polarized incident light of wavelength $\lambda = 488$ nm supplied by an argon-ion laser (Coherent Innova 90) operated at 500 mW or less. The intensity scale was calibrated against benzene. Measurements were made at angles of 90° to the incident beam. Dynamic light scattering (DLS) measurements were made under similar conditions by means of the Malvern instrument described above combined with a Brookhaven BI 9000 AT digital correlator. Measurements of scattered light were usually made at an angle of 90° to the incident beam. Experiment duration was in the range 5−20 min, and each experiment was repeated two or more times. The applicability of these methods to micellar solutions of the type under investigation has been discussed recently, *e.g.*, in refs 6−8.

The correlation functions from dynamic light scattering (DLS) were analyzed by the constrained regularized CONTIN method[16] to obtain distributions of decay rates (Γ). The distributions of decay rates were tested against changes in the regularizer and were found to be stable. The decay rates gave distributions of apparent diffusion coefficient ($D_{app} = \Gamma/q^2$) and hence of apparent hydrodynamic radius ($r_{h,app}$, radius of the hydrodynamically-equivalent hard sphere corresponding to D_{app}) *via* the Stokes−Einstein equation

$$r_{h,app} = kT/(6\pi\eta D_{app}) \tag{1}$$

where k is the Boltzmann constant and η is the viscosity of water at temperature T.

The basis for analysis of static light scattering (SLS) was the Rayleigh−Gans−Debye equation in the form

$$I - I_s = K^* c M_w \tag{2}$$

where I is intensity of light scattered from solution relative to that from benzene, I_s is the corresponding quantity for the solvent, c is the concentration (in g dm^{-3}), M_w is the mass-average molar mass of the solute, and

$$K^* = (4\pi^2/N_A\lambda^4)\,(n_B^2/R_B)(dn/dc)^2 \tag{3}$$

where N_A = Avogadro's constant, n_B and R_B = refractive index and Rayleigh ratio of benzene, respectively, and dn/dc is the specific refractive index increment. Sources of the quantities necessary for the calculations have been given previously, *e.g.*, in refs 4, 6, and 10, together with values of dn/dc and its temperature increment.

3. E-Block-Length Distributions

Molar mass distributions for the anionic polymerization of ethylene oxide under conditions of slow initiation have been derived by Weibull and Nycander.[17] A Poisson number-fraction distribution is expected[18] for a polymerization in which all steps have equal probability, whereas the Weibull−Nycander distribution assumes an initiation reaction with a rate constant different from that of all other steps. With reference to the present system, the assumption is a rate of disappearance of EO in the second stage of copolymerization of B_8E_{41} regulated by

$$-d[EO]/dt = k_o[B^*][EO] + k_1[E^*][EO] \tag{4}$$

with the ratio $k_1/k_o > 1$. (The notation B* and E* denotes active species.) This results in a widened E-block-length distribution. In the second stage of the copolymerization of $E_{41}B_8$, in which

$$-d[BO]/dt = k_o[E^*][BO] + k_1[B^*][BO] \tag{5}$$

the initiation reaction is effectively instantaneous, the B block has a Poisson distribution.

A more general approach is possible, whereby the rate constants for each step differ.[19] This approach has been used by Farkas *et al.*[20] in a study of the alcohol-initiated anionic polymerization of ethylene oxide to show that the rate constants of successive steps rapidly converge to a common value, making the Weibull−Nycander assumption satisfactory for fairly long E-block lengths, although with a modified interpretation of the two rate constants.

Following Weibull and Nycander[17], the E-block-length distribution (number fraction of x-mers, n_x) is given by

$$n_x = \frac{a^{x-1}}{(a-1)^x}\left[b + (b^c)\sum \frac{1}{j!}\{(a-1)\ln(b)\}^j\right] \qquad (6)$$

where $a = k_1/k_o$, b is the mole fraction of B* unreacted, and the sum runs from $j = 0$ to $x - 1$. The unknowns are n_x and a. b is available from end-group analysis by NMR. A second equation relates a to b and the number-average E-block length (x_n, also available from NMR) and gives a value for a

$$a = \frac{x_n - 1 + b}{b - \ln(b) - 1} \qquad (7)$$

In order to obtain a reliable value of a, values of b were measured for a series of $E_mB_nE_m$ copolymers with short E-block lengths prepared under conditions identical to those used for the present copolymers. Application of eq 7 to these results led to an average value of $a = 13$ (see Table 2). Higher values ($a = 20-30$) were found by Nace *et al.*[11] for copolymerization of B_nE_m and $E_mB_nE_m$ copolymers under industrial conditions, *e.g.*, at higher temperatures than those used in the laboratory. Number-fraction distributions calculated for $x_n = 41$ are shown in Figure 2: the presence of a significant number fraction of chains with short E blocks in the distribution of copolymer B_8E_{41} (compared with that of $E_{41}B_8$) is clearly seen. The number-fraction of chains with no added E units (not shown in Figure 2) is $b = 0.017$: this component was not important since copolymer B_8E_{41} was purified by hexane extraction to remove any poly(oxybutylene).

Transformation of the ordinate to mass fraction of copolymer (w_x, including the B block) and the abscissa first to $\log_{10} M$ (M of the copolymer) and then *via* the GPC calibration to elution volume [V, as if the copolymers were poly(oxyethylene)] gave the calculated GPC curves shown in Figure 3a, which can be compared with the experimental GPC curves plotted on the same scale in Figure 3b. The experimental curves are broader than the calculated, as a result of instrumental spreading, but otherwise agreement between the two comparisons is excellent, so confirming the applicability of eqs 4 to 7 to the present copolymers.

4. Results and Discussion

In reporting the results, emphasis is placed on comparison of the association and adsorption behaviors of the two copolymers. Clouding was not a problem. In fact solutions of each copolymer were clear up to the highest temperatures measured (*ca.* 95 °C) and over a wide concentration range; *e.g.*, up to 70 wt %.

4.1. Micelle Radius from Dynamic Light Scattering. Measurements were made at 25, 35, 45, and 50 °C, and for nine concentrations in the range $3-100$ g dm^{-3}. Examples of intensity fraction distributions of $\log_{10} r_{h,app}$ are shown in Figure 4 for solutions of $E_{41}B_8$ at 45 °C. These are seen to be single-peaked, with maxima at 6−7 nm, characteristic of micelles, which can be taken as evidence of closed association to micelles across the concentration range investigated. Broadening of the distributions at low concentrations is an effect of the CONTIN analysis acting upon data of low precision caused by low scattering intensities. Broadening of the distributions at high concentrations and a shift of the peak to lower values of $r_{h,app}$ are both effects of intermicellar interaction. The effect of temperature on DLS from solutions of copolymer $E_{41}B_8$ is shown for three concentrations in Figure 5. Irrespective of concentration, an increase in temperature led to a narrowing of the distribution.

As expected,[4,10] similar results were obtained for copolymer B_8E_{41}. However, as illustrated in Figure 6, the intensity fraction distributions of $\log_{10} r_{h,app}$ found for micelles of copolymer B_8E_{41} were narrower than those found for micelles of copolymer $E_{41}B_8$, especially at 25 °C. This is attributed to a small fraction of unassociated molecules (unimers) in the solutions of copolymer $E_{41}B_8$. Small signals are typically unresolved by CONTIN analysis, and lead to broadened distributions. This effect was less significant in the results obtained for solutions of copolymer B_8E_{41}. The results plotted in Figure 6, which are for a midrange

TABLE 2: End-Group Analysis of $E_mB_nE_m$ Copolymers[a]

E-block length	b	a
35	0.032	14
16	0.118	12
12	0.209	14
9	0.240	12
7	0.336	15

[a] b = mole fraction of unreacted B ends. a = Weibull−Nycander parameter k_1/k_o (see text).

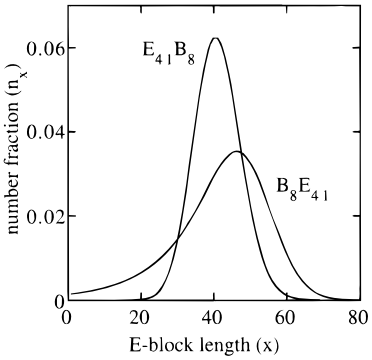

Figure 2. Number-fraction E-block-length distributions calculated according to Weibull and Nycander[17] for number-average E-block length $x_n = 41$, with $a = k_1/k_0 = 13$ for copolymer B_8E_{41}, and $a = 1$ (Poisson distribution) for copolymer $E_{41}B_8$.

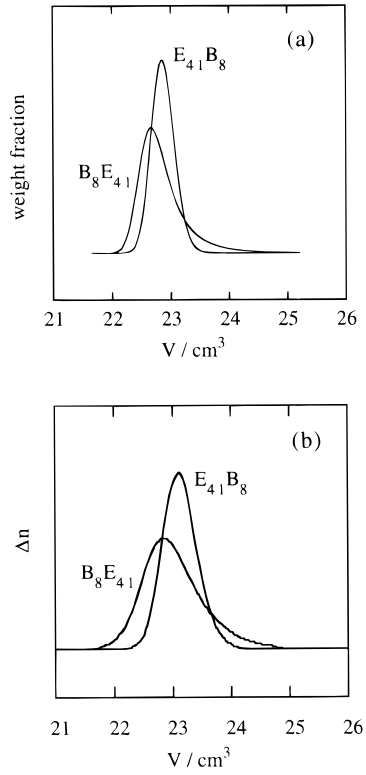

Figure 3. GPC curves for copolymers $E_{41}B_8$ and B_8E_{41} (as indicated). (a) Distributions calculated according to Weibull and Nycander[17] for number-average E-block length $x_n = 41$, and $a = k_1/k_o = 13$ for copolymer B_8E_{41}, and $a = 1$ (Poisson distribution) for copolymer $E_{41}B_8$, and transformed into GPC curves as outlined in the text. (b) Experimental GPC curves, including the effect of instrumental spreading.

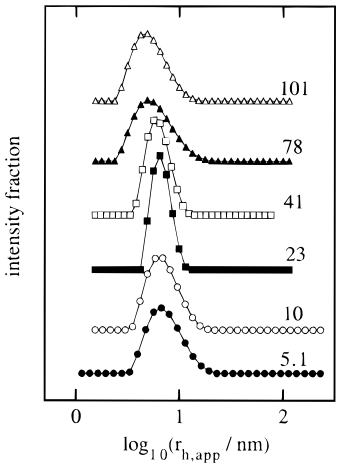

Figure 4. Dynamic light scattering from aqueous solutions of $E_{41}B_8$ at 45 °C with concentrations (in g dm^{-3}) indicated. The plots show intensity fractions of logarithmic apparent hydrodynamic radius, *i.e.*, $I(\log_{10} r_{h,app})$ *versus* $\log_{10} r_{h,app}$.

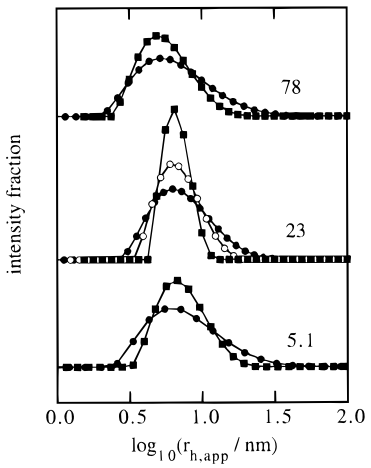

Figure 5. Effect of temperature on dynamic light scattering from aqueous solutions of $E_{41}B_8$ with the concentrations (in g dm^{-3}) indicated. The data points are for solutions at (●) 25, (○) 35, and (■) 45 °C. The plots show intensity fractions of logarithmic apparent hydrodynamic radius, *i.e.*, $I(\log_{10} r_{h,app})$ *versus* $\log_{10} r_{h,app}$.

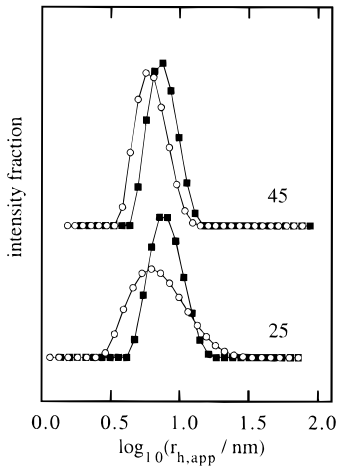

Figure 6. Dynamic light scattering from 40 g dm^{-3} aqueous solutions of copolymers (○) $E_{41}B_8$ and (■) B_8E_{41} at 25 and 45 °C (as indicated). The plots show intensity fractions of logarithmic apparent hydrodynamic radius, *i.e.*, $I(\log_{10} r_{h,app})$ *versus* $\log_{10} r_{h,app}$.

concentration ($c \approx 40$ g dm^{-3}), show again the effect of temperature on distribution width, and also indicate the larger size of the micelles of copolymer B_8E_{41} compared with those of copolymer $E_{41}B_8$.

Intensity-average values of $r_{h,app}$ (obtained by integrating over the distribution of decay rate using the CONTIN program) are plotted as $1/r_{h,app}$ against concentration in Figure 7. The quantity $1/r_{h,app}$ is proportional to the apparent diffusion coefficient D_{app} through the Stokes−Einstein equation (eq 1), but is compensated for changes in solvent viscosity and temperature, so allowing direct comparison of results obtained for solutions at more than one temperature. The increase in $1/r_{h,app}$ with concentration (*i.e.*, the increase in D_{app}) seen in Figure 7 for both copolymers is characteristic of micelles acting as hard spheres. It is clear that values of $1/r_{h,app}$ are systematically higher for micelles of copolymer B_8E_{41} compared with $E_{41}B_8$.

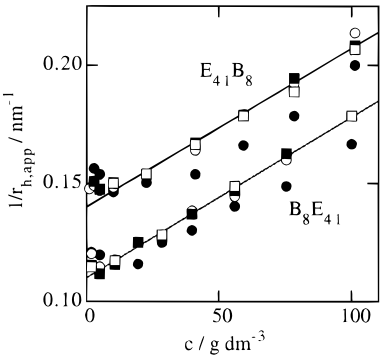

Figure 7. Inverse apparent hydrodynamic radius of micelles *versus* concentration for aqueous solutions of $E_{41}B_8$ and B_8E_{41} (as indicated). The data points are for solutions at (●) 25, (○) 35, and (■) 45, and (□) 50 °C.

TABLE 3: Micellar Hydrodynamic Properties from Dynamic Light Scattering

	$E_{41}B_8$			B_8E_{41}		
T/°C	$10^{11}D$/m^2 s^{-1}	r_h/nm	δ_h	$10^{11}D$/m^2 s^{-1}	r_h/nm	δ_h
25	3.3	7.5	21	2.6	9.3	16
35	4.4	7.2	13	3.5	9.0	11
45	5.5	7.1	10	4.3	9.2	10
50	6.1	7.1	9	4.8	9.1	9

The plots turn upward at very low concentrations, an effect which is most apparent for copolymer $E_{41}B_8$ at low temperatures, but is also seen for copolymer B_8E_{41}. This is a further manifestation of micellar dissociation. The results for solutions at 25 °C are affected by dissociation up to relatively high concentrations, consistent with the negative temperature coefficient of solubility in the systems. Under these circumstances, values of r_h for the micelles at zero concentration were obtained by fitting the higher-concentration data points to straight lines (by least squares) and extrapolating to zero concentration: *i.e.*, $c \geq 10$ g dm^{-3} for $T \geq 35$ °C; $c \geq 20$ g dm^{-3} for $T = 25$ °C. As can be seen in Figure 7, the data points for solutions of a given copolymer at $T \geq 35$ °C fitted to the same straight lines, so yielding identical values of $r_{h,app}$.

Values of r_h and D (zero concentration) are listed in Table 3, together with values of the hydrodynamic swelling factor, δ_h, which is defined as the hydrodynamic volume ($v_h = (4/3)\pi r_h^3$) divided by the anhydrous volume v_a: *i.e.*, $v_a = M_w/N_A\rho$, where M_w is the mass-average molar mass of the micelles determined by static light scattering (see section 4.3), N_A is Avogadro's constant, and ρ is the density of anhydrous copolymer, approximated by 1.07 g cm^{-3} for the temperature range under consideration.

The weak temperature dependence of hydrodynamic radius is a well-established result for block copolyether micelles in aqueous solution, and was explained many years ago[21] as a consequence of compensation between an increase in association number (see section 4.3) and a decrease in swelling of the micellar fringe (essentially δ_h) as temperature is increased. For

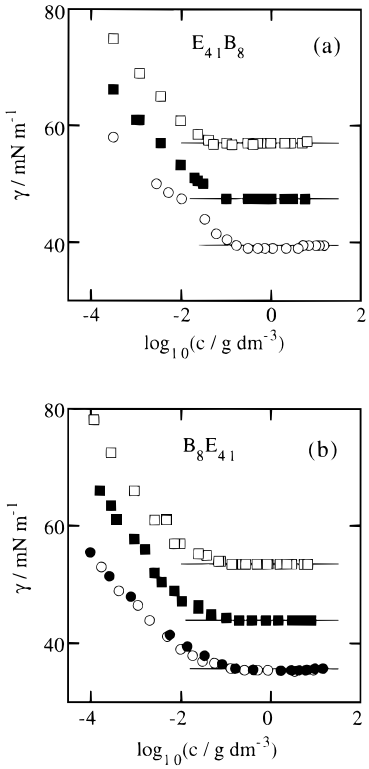

Figure 8. Surface tension (γ) *versus* logarithm of concentration for aqueous solutions of (a) $E_{41}B_8$ and (b) B_8E_{41} (●) 26, (○) 30, (■) 40, and (□) 50 °C. For clarity, the data points for solutions at 40 and 50 °C are displaced by +10 and +20 mN m^{-1} respectively.

the present copolymers, this principle holds well at $T \geq 35$ °C, but breaks down at the lower temperature.

4.2. Critical Micelle Concentration from Surface Tension. Plots of surface tension against logarithm of concentration are shown in Figure 8. There is a clear difference between the results for the two copolymers: the curves for solutions of $E_{41}B_8$ show a sharp break which can be assigned to the critical micelle concentration (cmc) while those for B_8E_{41} curve continuously toward a constant value. Moreover, as noted previously,[10] the $\gamma-\log(c)$ curves for solutions at the lowest temperatures show shallow minima before reaching a constant value of γ. This last effect (more noticeable for $E_{41}B_8$) is assigned to the selective adsorption at low concentrations of surface active, poorly soluble components, followed by their solubilization in micelles at concentrations significantly above the cmc. These components were probably chains with very short E blocks in copolymer B_8E_{41} (see section 3) or a residue of hydroxy-ended poly(oxybutylene) not removed by hexane extraction in copolymer $E_{41}B_8$. The latter contention was confirmed by determining a $\gamma-\log(c)$ curve for an unpurified sample of $E_{41}B_8$ and noting a deeper minimum. Effects of this type have been described for other E/B copolymers[22] and for other types of surfactant.[23] The curvature of the plots found for solutions of copolymer B_8E_{41} at all temperatures must also originate in the wide distribution of E-block lengths in that sample. The fall in γ reflects the packing of adsorbed copolymer in the Gibbs surface monolayer, which is clearly distribution dependent. This effect is discussed in section 4.4.

For present purposes it is necessary to define the cmc, and we take this to be the point at which the surface tension reaches its constant value, *i.e.*, when the Gibbs monolayer is full. For those $\gamma-\log(c)$ curves which showed a minimum (*i.e.*, B_8E_{41}, ≤ 30 °C), the cmc was taken to be the concentration at the minimum. Both these procedures were consistent with previous practice.[4,14,22] Values of the cmc are listed in Table 4. Comparison is made with previous measurements[10] for copolymer B_8E_{41}, and the results are seen to agree within the uncertainty of the experiments. The logarithm of cmc is plotted against reciprocal temperature in Figure 9. The derivation of thermodynamic quantities from these results is described in section 4.5.

TABLE 4: Surface Tension: Values of cmc and γ_{cmc}[a]

	$E_{41}B_8$			B_8E_{41}	
T/°C	cmc/ g dm^{-3}	a_{cmc}/ nm^2	γ_{cmc}/ mN m^{-1}	cmc/ g dm^{-3}	γ_{cmc}/ mN m^{-1}
25[b]	(0.6)			(1.0)	
26				0.9	35.7
28[c]				0.9	35.7
30	0.35	1.4	39.5	0.8	35.5
40	0.11	1.2	37.5	0.21	34.0
40[c]				0.3	33.0
50	0.05	1.1	37.0	0.13	33.5

[a] Estimated uncertainty in cmc ±20%. [b] Values in parentheses obtained by extrapolation: see Figure 9. [c] Values from ref 10.

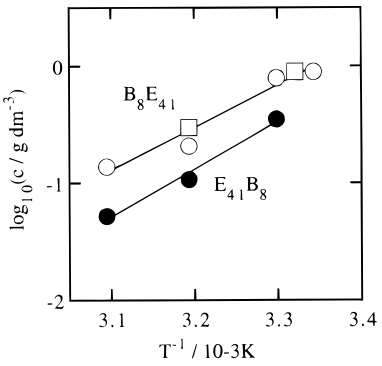

Figure 9. Critical micelle concentrations from surface tension measurements for aqueous solutions of copolymers $E_{41}B_8$ and B_8E_{41}. Logarithm of cmc *versus* inverse temperature for (●, ○) present results and (□) previous results (ref 4). The straight line is the least-squares fit to all data points.

4.3. Micelle Mass and Radius from Static Light Scattering. For a nonideal, dilute solution of micelles, the Debye equation can be written as

$$K^*c'/(I - I_{cmc}) = 1/M_w + 2A_2c' + ... \qquad (8)$$

where c' is the concentration of micelles (in g dm^{-3}) equal to the total copolymer concentration minus the cmc (*i.e.*, $c' = c - \text{cmc}$), I_{cmc} is the intensity of scattering from unimer solution (*i.e.*, copolymer solution at the cmc), M_w is the mass-average molar mass of the micelles, and A_2 is the second virial coefficient (higher terms being omitted from eq 8) reflecting the interaction of the micelles in solution. As written, the equation assumes small particles relative to the wavelength of the light. In this respect, within the concentration ranges where the copolymers were essentially entirely micellized the dissymmetry ratio (I_{45}/I_{135}) was consistently near unity for solutions of both copolymers.

In principle, using eq 8 truncated to the second term yields values of M_w and A_2 *via* a linear extrapolation. In practice that procedure was not satisfactory, particularly for solutions of copolymer $E_{41}B_8$ at the lowest temperature. This is illustrated in Figure 10, which shows two Debye plots for copolymer $E_{41}B_8$, one constructed using the actual copolymer concentration and the other using the corrected (micelle) concentration $c' = (c - \text{cmc})$, with the cmc taken from Figure 9. The upturn in the uncorrected Debye function at low concentrations is a result of micellar dissociation. As can be seen in Figure 10, correction using the cmc obtained by surface tension does not wholly compensate for this effect. The use of I_{cmc} in place of I_s, a small adjustment, makes matters worse (see, *e.g.*, ref 7). This

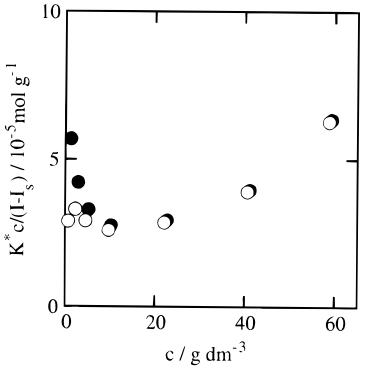

Figure 10. Debye plots for aqueous solutions of $E_{41}B_8$ at 25 °C: (●) using the actual copolymer concentration, c; (○) using the corrected copolymer concentration, $c' = (c - \text{cmc})$.

divergence between the cmc from surface tension and the requirement for correction of the Debye function to obtain a linear extrapolation to zero concentration has been discussed and explained previously.[6]

In recent work in Manchester the problem of micellar dissociation has been circumvented by adopting a suggestion of Vrij[24] and extrapolating to zero concentration from the moderate concentration range guided by the Carnahan−Starling equation,[25] which is equivalent to the virial expansion for the structure factor for hard spheres taken to its seventh term. In this procedure, the interparticle interference factor (structure factor, S) in the scattering equation

$$K^*c'/(I - I_s) = 1/SM_w \tag{9}$$

is approximated by

$$1/S = [(1 + 2\phi)^2 - \phi^2(4\phi - \phi^2)](1 - \phi)^{-4} \tag{10}$$

where ϕ is the volume fraction of equivalent uniform spheres. In practice, values of ϕ were calculated from the volume fraction of micelles in the system by applying a thermodynamic expansion factor δ_t, *i.e.*, the ratio of the thermodynamic volume (v_t) to anhydrous volume (v_a) (where the thermodynamic volume is one-eighth of the excluded volume):

$$\delta_t = v_t/v_a \tag{11}$$

In an approximate treatment, concentrations were converted to volume fractions assuming a density of dry polymer of $\rho \approx 1.07$ g dm^{-3} irrespective of temperature. In principle, the concentration used to calculate ϕ should be $c' = (c - \text{cmc})$: in practice it sufficed to use c itself, since the correction was negligible in the moderate concentration range (see Figure 10). Fitting eqs 9 and 10 to the data gave values of M_w and δ_t. Application of the procedure to the scattering intensities from aqueous solutions of copolymer $E_{41}B_8$ is illustrated in Figure 11. Similar plots have been published for aqueous solutions of copolymer B_8E_{41}.[4,10] As discussed previously[4,10] and confirmed in present work, the effect of micellar dissociation of B_8E_{41} micelles was seen only at extremely low concentrations, which is an effect of its wide E-block-length distribution.

Values of M_w and δ_t are listed in Table 5, together with association numbers of the micelles calculated from

$$N_w = M_w(\text{micelle})/M_w(\text{molecule}) \tag{12}$$

using values of M_w(molecule) listed in Table 1, and values of the thermodynamic radii calculated from the thermodynamic volume. Comparison with values obtained previously for micelles of copolymer B_8E_{41}[4,10] shows satisfactory agreement.

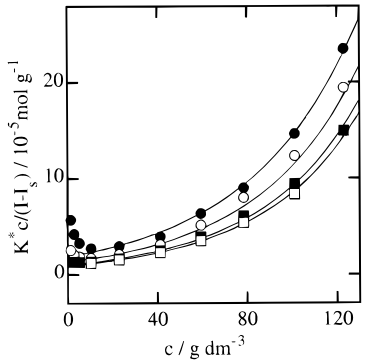

Figure 11. Debye plots for aqueous solutions of $E_{41}B_8$ at (●) 25, (○) 35, (■) 45 and (□) 50 °C. Concentrations are uncorrected. The curves were calculated using eqs 9 and 10.

TABLE 5: Micellar Characteristics from Static Light Scattering

	$E_{41}B_8$				B_8E_{41}			
T/°C	$10^{-5}M_w$/ g mol^{-1}	N_w	r_t/nm	δ_t	$10^{-5}M_w$/ g mol^{-1}	N_w	r_t/nm	δ_t
25	0.53	21	3.8	2.8	1.4	52	5.7	3.6
25[a]					1.5	58	6.0	3.8
35	0.75	30	4.3	3.0	1.8	66	6.3	3.7
45	0.99	40	4.8	3.1	2.2	81	6.6	3.7
50[a]					2.3	85	6.9	3.8
50	1.1	44	4.9	3.1	2.3	85	6.8	3.7

[a] Values from ref 10.

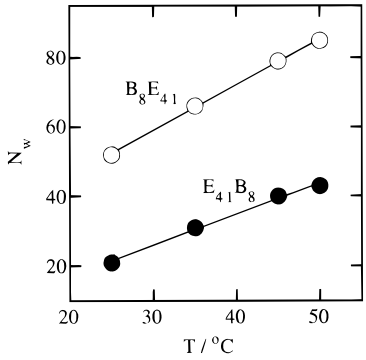

Figure 12. Plots of micellar aggregation number (N_w) *versus* temperature for aqueous solutions of copolymers (●) $E_{41}B_8$ and (○) B_8E_{41}.

It is noted that the association numbers of the micelles increased linearly with temperature for both copolymers: see Figure 12.

The larger association numbers and thermodynamic radii found for micelles of copolymer B_8E_{41} (see Table 5 and Figure 12) are consistent with their larger hydrodynamic radii determined by DLS (see Table 3). Since the B blocks have essentially identical average lengths and length distributions (Poisson), then the difference must lie with the different E-block-length distributions in the two copolymers. This point is discussed in section 4.5.

4.4. Effect of E-Block-Length Distribution on Adsorption at the Air−Water Interface. Because of curvature in the plots of γ *versus* log(cmc) determined for copolymer B_8E_{41} (see Figure 8), with consequent uncertainty in determining slopes below the cmc, it was not possible to obtain[26] unique values of the area per molecule in the surface monolayer just below the cmc (a_{cmc}). Because of this, no values of a_{cmc} are quoted for B_8E_{41} in Table 4. The qualitative impression from comparison with corresponding plots for copolymer $E_{41}B_8$ (see Figure 8) is that the area per molecule did not differ greatly between the two systems at low concentrations; *i.e.*, any differences in adsorption behavior were confined to the concentration region very near the cmc, where the surface monolayer is almost full.

TABLE 6: Standard Thermodynamic Quantities of Micellization

copolymer	$\Delta_{mic}G°$(40 °C) kJ mol^{-1}	$\Delta_{mic}H°$(26−50 °C) kJ mol^{-1}	$T\Delta_{mic}S°$(40 °C) kJ mol^{-1}
$E_{41}B_8$	−26.0	78	104
B_8E_{41}	−24.8	70	95

Values of a_{cmc} were obtained for copolymer $E_{41}B_8$, as listed in Table 4. These values (1.0−1.4 nm^2) are larger than those reported previously[22] for aqueous solutions of E_mB_n copolymers: *e.g.,* 0.5−0.9 nm^2. This may be related to sample purity,[22] or to the longer equilibration times allowed in the present experiments for solutions of low concentration (*e.g.,* up to 2 days compared with 1 day[22]). Considering the results in Table 4, the effect of an increase in temperature in reducing the value of a_{cmc} is consistent with a reduction in the E-block coil dimensions caused by water being a poorer solvent at high temperature.

A quantity which can be precisely derived for both copolymers is the surface tension of the full monolayer above the cmc (γ_{cmc}); see Table 4. Values of γ_{cmc} were systematically lower for solutions of copolymer B_8E_{41} compared to $E_{41}B_8$. Correlation of a_{cmc} with γ_{cmc} is well established for nonionic surfactants, *e.g.,* for uniform and nonuniform alcohol and octyl phenol ethoxylates,[27−29] and the lower values of γ_{cmc} found for solutions of B_8E_{41} can be taken as evidence of lower values of a_{cmc}.

Crook *et al.*[27] have reported a comparison of the surface properties of uniform and nonuniform oxyethylene adducts of octylphenol. They found that solutions of the samples with nonuniform E blocks had lower values of γ_{cmc}. An adequate explanation of those and present results is preferential adsorption of those molecules in the distribution which have short E blocks,[27] which, in the present case, favors adsorption of copolymer B_8E_{41}. The underlying effect of E-block length on a_{cmc} and γ_{cmc} is well established for $E_mP_nE_m$ copolymer surfactants[30,31] as well as the oxyethylene adducts referred to above.[27−29]

Preferential adsorption effects have been described for copolymer B_8E_{41} on hydrophobic solid surfaces,[12] the strong preference being for adsorption of chains with long B blocks, with a weaker preference for chains with short E blocks. Polydispersity was seen to lead to adsorption isotherms characteristic of high affinity. The surface excess concentrations ($\Gamma = M_n/N_A a$) found for the two systems are 2.8 mg m^{-2} (present work, $E_{41}B_8$, air−water interface, 30 °C) and 1.8 mg m^{-2} (ref 12, B_8E_{41}, hydrophobic surface, value at high solute concentration, 25 °C). We suspect that this difference is caused by the difference in the surfaces .

4.5. Effect of E-Block-Length Distribution on Micellization and Micelle Properties. The results from surface tension measurements presented in section 4.2 show similar (though not identical) values of the cmc for the two copolymers. If the approximate equations[32] for the standard Gibbs energy and standard enthalpy of micellization are adopted, *i.e.,*

$$\Delta_{mic}G° = RT \ln(\text{cmc}) \quad (\text{cmc in mol dm}^{-3}) \qquad (13)$$

and

$$\Delta_{mic}H° = R\,(\mathrm{d} \ln(\text{cmc})/\mathrm{d}(1/T)) \qquad (14)$$

then the present data (see Figure 9) give the standard thermodynamic quantities (including the standard entropy of micellization) listed in Table 6. The standard states are copolymer molecules in ideally dilute solution (c = 1 mol dm^{-3}) and copolymer molecules in micelles, and the values are per mole of copolymer molecules. Similar values of $\Delta_{mic}H°$ have been found for other E/B block copolymers with fairly short B blocks: *e.g.,* 80 kJ mol^{-1} ($E_{27}B_7$, $E_{30}B_5$),[33] 95 kJ mol^{-1} ($E_{21}B_8E_{21}$),[2] and 80 kJ mol^{-1} ($B_5E_{91}B_5$).[5]

The similarity of the values of all three standard quantities found for the two copolymers reflects the similarity of their B-block lengths and length distributions, coupled with the fact that it is the hydrophobic block (hence the hydrophobic effect) which dominates the micellization process. The E-block-length distribution can cause only a minor perturbation of the overall effect, and this is seen to be so.

The overall micellization process depends on the standard Gibbs energy change. It is known from previous work[2,10] that the incremental change in $\Delta_{mic}G°$ per B unit is about 2.3 kJ mol^{-1} at 40 °C (*i.e.,* similar to that per C unit of C_nE_m surfactants). This being so, the difference in the values of $\Delta_{mic}G°$ found for the two copolymers, 1.2 kJ mol^{-1} at 40 °C, is simply that expected for a difference in average B-block length of half of one unit, which is the uncertainty in the determination of the difference in block lengths. Accordingly, we have not tried to interpret the small differences seen in Table 6.

The results from dynamic and static light scattering (Tables 3 and 5) show that the micelles formed in aqueous solutions of copolymer B_8E_{41} are larger in all respects (r_h, r_t, N_w) than those formed from copolymer $E_{41}B_8$ under identical conditions. These results relate to micelles at concentrations and temperatures well removed from their critical values. For N_w in particular, which is 40 for $E_{41}B_8$ micelles in solution at 45 °C but 81 for B_8E_{41} micelles under comparable conditions, the effect is well outside possible experimental error.

The B-block-length distribution is essentially the same in the two copolymers, and any effects of small differences in the average and distribution should be small, since previous correlations indicate an increase in N_w of only (approximately) 10 for each extra unit in the B block.[2,6]

Considering the association numbers measured for each copolymer in solution at 45 °C, and assuming spherical micelles, core radii are estimated to be 2.1 nm ($E_{41}B_8$) and 2.6 nm (B_8E_{41}). Since the fully stretched (all-trans) length of a B_8 block is approximately 3.0 nm, it is seen that spherical micelles may be formed in either case, though with more chain stretching (on average) of the B blocks in the cores of the B_8E_{41} micelles. The assumption of micelle sphericity is supported by calculation of the area per molecule passing through the core−fringe interface of the micelles, which is simply derived from the core radius and the association number. The values obtained are 1.4 nm^2 for $E_{41}B_8$ micelles and 1.1 nm^2 for B_8E_{41} micelles., *i.e.,* comparable with the values of the area per molecule in the surface monolayer (a_{cmc}) listed in Table 4.

As discussed in section 4.4, differences in adsorption at the air−water interface can be explained by preferential adsorption of the more hydrophobic molecules in the distribution, *i.e.,* in the present case those with short E blocks. It is probable that the same molecules preferentially micellize. Regarding association number, previous evidence is that copolymers with short E blocks form large micelles: compare, for example, N_w = 70 for $E_{24}B_{10}$ at 30 °C,[22] N_w = 60 for $E_{32}B_{10}$ at 30 °C,[33] and N_w = 37 for $E_{40}B_{10}$ at 30 °C.[34] Present results from dynamic light scattering (see section 4.1, Figure 6) indicate that the effect of preferential micellization may be to narrow the micelle size distribution at the expense of the smaller micelles. It is possible that a more subtle effect of E-block-length distribution regulates micelle size. The larger size of the B_8E_{41} micelles may be a consequence of a difference in conformation of the E blocks in the micelle fringe, the short and long E blocks contained in the distribution of B_8E_{41} being accommodated with less overall

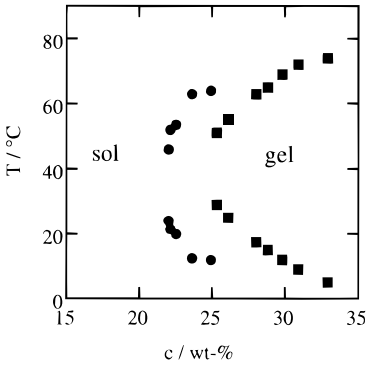

Figure 13. Sol−gel boundaries determined by tube inversion for aqueous solutions of copolymers (●) $E_{41}B_8$ and (■) B_8E_{41}. The data are from refs 4 and 13.

stretching than the more uniform E blocks in $E_{41}B_8$. A related effect has been explored theoretically for polydisperse nonadsorbing blocks in adsorbed surface layers of copolymers,[35] and has been described and discussed for adsorbed surface layers of B_8E_{41}.[12]

4.6. Gel−Sol Diagrams. Figure 13 shows gel−sol boundaries for solutions of the two copolymers in the concentration range 20−40 wt % copolymer. The results, established by a tube-inversion method, are taken from recent reports,[4,13] and cover the isotropic gel region of the phase diagram. It is seen that the critical gel concentrations found for solutions of copolymer B_8E_{41} at given temperatures are systematically lower than those found for solutions of copolymer $E_{41}B_8$.

Assuming that the isotropic gels are cubic phases in which the micelles acting as hard spheres pack together, as shown directly for micelles of $E_mP_nE_m$ copolymers by SANS,[36,37] then the sol−gel boundary will occur when the volume fraction of hard spheres in the system (ϕ) reaches a critical value. This can be taken as $\phi_c \approx 0.7$ for packed spheres forming a cubic structure. An appropriate measure of the hard sphere volume, accessible from SLS measurements on dilute solutions, is the thermodynamic volume (v_t) which relates to the collision radius of the excluded sphere. If the thermodynamic expansion factor (δ_t, defined by eq 11) is obtained directly from light scattering, then the critical gelation concentration (cgc in g dm^{-3}) can be calculated from

$$\text{cgc} = 1000\phi_c\rho/\delta_t \qquad (15)$$

With $\phi_c = 0.7$, and taking values of δ_t of micelles in solution at 35 °C from Table 5 (*i.e.*, $\delta_t = 3.1$ for $E_{41}B_8$ and $\delta_t = 3.7$ for B_8E_{41}), and assuming $\rho \approx 1.07$ g cm^{-3}, the calculated critical gelation concentrations at 35 °C are 242 and 202 g dm^{-3} for copolymers $E_{41}B_8$ and B_8E_{41}, respectively, which convert to 25 and 20 wt %, compared with observed values (see Figure 13) of 25 and 21 wt %, respectively.

The possibility of using the thermodynamic (exclusion) parameters derived from dilute measurements to predict gelation of concentrated solutions of spherical micelles has been discussed in detail previously.[34] In the present case, the difference in cgc is seen to originate in the different exclusion properties of the micelles. Since the micelle core is very small in volume compared to the fringe, this effectively means the different exclusion properties of the E-block fringes of the micelles. The useful feature of the thermodynamic expansion factor, δ_t, as distinct from r_t or r_h, is that it is independent of N_w, hence a significant difference in δ_t translates directly to a significant difference in the exclusion properties of the fringe. The present results show that a wider E-block-length distribution leads to a larger exclusion effect, no doubt because of the presence of longer E blocks in the distribution.

Acknowledgment. We thank Dr. Frank Heatley and Mr. Keith Nixon for help with the NMR and GPC. Prof. Provencher kindly provided a copy of the CONTIN program. Financial assistance was provided by EPSRC and BBSRC. Our reviewer made valuable suggestions which improved the discussion.

References and Notes

(1) Dow Chemical Co., Freeport, TX, Technical Literature; *B-Series Polyglycols. Butylene Oxide/Ethylene Oxide Block Copolymers*, 1994.

(2) Yang, Y.-W.; Deng, N.-J.; Yu, G.-E.; Zhou, Z.-K.; Attwood, D.; Booth, C. *Langmuir* **1995**, *11*, 4703.

(3) *Nonionic Surfactants, Polyoxyalkylene Block Copolymers*; Nace, V. M., Ed.; Surfactant Science Series 60; Marcel Dekker: New York, 1996.

(4) Yang, Z.; Pickard, S.; Deng, N.-J.; Barlow, R. J.; Attwood, D.; Booth, C. *Macromolecules* **1994**, *27*, 2371.

(5) Yang, Y.-W.; Yang, Z.; Zhou, Z.-K.; Attwood, D.; Booth, C. *Macromolecules* **1996**, *29*, 670.

(6) Yu, G.-E.; Yang, Y.-W.; Yang, Z.; Attwood, D.; Booth, C.; Nace, V. M. *Langmuir* **1996**, *12*, 3404.

(7) Yu, G.-E.; Yang, Z.; Attwood, D.; Price, C.; Booth, C. *Macromolecules* **1996**, *29*, 8497.

(8) Yu, G.-E.; Zhou, Z.-K.; Attwood, D.; Price, C.; Booth, C.; Griffiths, P. C.; Stilbs, P. *J. Chem. Soc., Faraday Trans.* **1996**, *92*, 5021.

(9) Nace, V. M. *J. Am. Oil Chem. Soc.* **1996**, *73* , 1.

(10) Yang, Z.; Yang, Y.-W.; Zhou, Z.-K.; Attwood, D.; Booth, C. *J. Chem. Soc., Faraday Trans.* **1996**, *92*, 257.

(11) Nace, V. M.; Whitmarsh, R. H.; Edens, M. W. *J. Am. Oil Chem. Soc.* **1994**, *71*, 777.

(12) Schillen, K; Claeson, P. M.; Malmsten, M.; Linse, P.; Booth, C. *J. Phys. Chem. B* **1997**, *101*, 4238.

(13) Li, H.; Yu, G.-E.; Price, C.; Booth, C.; Hecht, E.; Hoffman, H. *Macromolecules* **1997**, *30*, 1347.

(14) Reddy, N. K. ; Fordham, P. J.; Attwood, D.; Booth, C. *J. Chem. Soc., Faraday Trans.* **1990**, *86*, 1569.

(15) Heatley, F.; Yu, G.-E.; Sun, W. -B.; Pywell, E. J.; Mobbs, R. H.; Booth, C. *Eur. Polym. J.* **1990**, *26*, 583.

(16) Provencher, S. W. *Makromol. Chem.* **1979**, *180*, 201.

(17) Weibull, B.; Nycander, B. *Acta Chem. Scand.* **1954**, *8*, 847.

(18) Flory, P. J. *J. Am. Chem. Soc.* **1945**, *62*, 1561.

(19) Natta, G. E.; Mantica, J. *J. Am. Chem. Soc.* **1952**, *74*, 3152.

(20) Farkas, L.; Morgos, J.; Sallay, P.; Rusznak, I.; Bartha, B.; Veress, G. *J. Am. Oil Chem. Soc.* **1981**, *58*, 650.

(21) Attwood, D.; Collett, J. H.; Tait, C. J. *Int. J. Pharm.* **1985**, *26*, 25.

(22) Bedells, A. D.; Arafeh, R. M.; Yang, Z.; Attwood, D.; Heatley, F.; Padget, J.C.; Price, C.; Booth, C. *J. Chem. Soc., Faraday Trans.* **1993**, *89*, 1235.

(23) Rosen, M. J. *J. Colloid Interface Sci.* 1981, **79**, 587.

(24) Vrij, A. *J. Chem. Phys.* **1978**, *69*, 1742.

(25) Carnahan, N. F.; Starling, K. E. *J. Chem. Phys.* **1969**, *51*, 635.

(26) Attwood, D.; Florence, A. T. *Surfactant Systems*; Chapman and Hall: London, 1983; p 14.

(27) Crook, E. H.; Fordyce, D. B.; Trebbi, G. F. *J. Phys. Chem.* **1963**, *67*, 1987.

(28) Rosen, M. J.; Cohen, A. W.; Dahanayake, M.; Hua, X.-Y. *J. Phys. Chem.* **1982**, *86*, 541.

(29) Reddy, N. K.; Foster, A.; Styring, M. G.; Booth, C. *J. Colloid Interface Sci.* **1990**, *136*, 588.

(30) Alexandridis, P.; Athenassiou, V.; Fukuda, S.; Hatton, T. A. *Langmuir* **1994**, *10*, 2604.

(31) Chu, B; Zhou, Z.-K. In ref 3, Chapter 3.

(32) Attwood, D.; Florence, A. T. *Surfactant Systems*; Chapman and Hall: London, 1983; p 101.

(33) Tanodekaew, S.; Deng, N.-J.; Smith, S.; Yang, Y.-W.; Attwood, D.; Booth, C. *J. Phys. Chem.* **1993**, *97*, 11847.

(34) Deng, N.-J.; Luo, Y.-Z.; Tanodekaew, S.; Bingham, N.; Attwood, D.; Booth, C. *J. Polym. Sci., Part B, Polym. Phys.* **1995**, *33*, 1085.

(35) Dan, N.; Tirrell, M. *Macromolecules* **1993**, *26*, 6467.

(36) Mortensen, K.; Pedersen, J. S. *Macromolecules* **1993**, *26*, 805.

(37) Mortensen, K.; Brown, W.; Nordén, W. *Phys. Rev. Lett.* **1992**, *68*, 2340.